International Journal of Coal Geology 159 (2016) 71–81

Contents lists available at ScienceDirect

International Journal of Coal Geology

journal homepage: www.elsevier.com/locate/ijcoalgeo

An analytical method for modeling and analysis gas-water relative permeability in nanoscale pores with interfacial effects

Tianxin Li [a], Hongqing Song [a,b,*], Jiulong Wang [a], Yuhe Wang [c], John Killough [b]

[a] School of Civil and Environmental Engineering, University of Science and Technology Beijing, China
[b] Department of Petroleum Engineering, Texas A&M University, TX, USA
[c] Department of Petroleum Engineering, Texas A&M University at Qatar, Qatar

ARTICLE INFO

Article history:
Received 2 November 2015
Received in revised form 29 March 2016
Accepted 30 March 2016
Available online 9 April 2016

Keywords:
Analytical model
Gas-water relative permeability
Nanoscale pores
Interfacial effects
Shale gas

ABSTRACT

This paper provides an analytical method for modeling and analyzing gas-water relative permeability in nanoscale pores with interfacial effects in terms of Hagen Poiseuille formula and capillary pressure curve. The flow models considering the interfacial effects in nanoporous shows good agreements with experimental data comparing with other models. The changing characteristics of gas-water relative permeability were analyzed under different conditions such as nanotube radius, film thickness, surface diffusion and contact angle. The results show that the larger the nanotube radius, the greater the relative permeability values because of decreasing both interfacial microstructure effect and the resistance of fluid flow. With the increasing of film thickness, surface diffusion which is positive for flow decreases in nanoscale pores. When the contact angle >90° solid interface repel water and the hydrophobic of surfaces reduce the resistance to fluid flow, and the gas-water relative permeability increases with increasing contact angle. On the contrary when contact angle <90°, the solid interface shows hydrophilic properties which play a negative effect to the fluid flow. This study has provided a new insight and theoretical basis for development of shale gas reservoirs with nanoscale pores.

1. Introduction

With the increase of world energy demand, unconventional oil and gas resources play an important role in the global energy structure such as shale gas and tight gas. The characteristics of shale gas reservoir are low porosity, low/ultra-low permeability, and containing nanoscale pores. For example, the Mississippian Barnett Shale basin, the reservoir pore size range is 5–750 nm, and the average pore size is 100 nm (Yang, F. et al., 2013). The fracture network of shale gas reservoir is formed by hydraulic fracturing to improve the flow capacity of shale gas in industrial production. Up to now, about 85% of US production of shale gas wells used horizontal wells and multi-stage fracturing technology (Haifeng, Z. et al., 2012). The fracture network is the main gas flow passage in the shale gas production process which artificial fracture width is generally in the 500 nm–50 μm and entire fracture network scales across 50 nm–50 μm (Yang, F. et al., 2013).

According to Knudsen number, gas flow can be divided into four kinds of flow regime: continuous flow ($Kn < 10^{-3}$), slip flow ($10^{-3} < Kn < 0.1$), transition flow ($0.1 < Kn < 10$) and Knudsen flow ($Kn > 10$) (Beskok, A. et al., 1996). The reason of different flow regimes is interfacial effects essentially. When the tube diameter is large, the flow regime of gas mainly belongs to continuous flow, just only show up slip flow regime near the tube wall (Ozkan, E. et al., 2010). However Knudsen flow and transitional flow are the most important flow regimes that cause the strong interfacial effects in nanotubes. Therefore, single phase fluid flow in nanoscale pores should consider the interfacial effects.

Because of the existence of initial water and fracturing fluid in shale gas reservoir, there is obvious gas and water two-phase flow in the shale production (Haifeng, Z. et al., 2012), but otherwise, there is a big difference between the flow pattern of two-phase flow and single gas flow. And it cannot determine the two phase flow regime that only relies on Knudsen number. The research on relative permeability of gas and water phase in fracture network of shale gas reservoir with nanoscale pores is very important for shale gas production.

There is little research on relative permeability of gas and water phase in fracture network with nanoscale pores with interfacial effects currently. However there are some theoretical and experimental research results on two-phase relative permeability without interfacial effects. On the one hand, in terms of theoretical research, the primary study on the relative permeability in natural fractures is Romm's model or X model (Romm 1966), which assumed no phase interference existence between two phases. So the X-model is too idealistic to describe relative permeability as functions of saturation. Then, Brooks (1966) proposed a semi-empirical model based on Corey model (Corey, 1954) and tortuosity-saturation function, which could be called

* Corresponding author at: 30 Xueyuan road Haidian District Beijing, China.
E-mail address: songhongqing@ustb.edu.cn (H. Song).

http://dx.doi.org/10.1016/j.coal.2016.03.018
0166-5162/

the Brooks–Corey model. And it has been widely used for modeling two-phase relative permeability. Fourar and Lenormand (1998) derived viscous-coupling model, which is a new analytical model considering the influence of viscosity from Stokes' equation. Chima and Geiger (2012) also proposed an analytical model of relative permeability, based on shell momentum balance, Newton's law of viscosity and cubic law for flow in fractures (Fig. 1). When ignoring the capillary force, Chima's model could be transformed into viscous-coupling model. The details of relative permeability models are given in Appendix A. On the other hand, in terms of experimental research, Persoff and Pruess (1995) studied the rules of gas-water relative permeability through natural fracture cores, the results show that the rules of relative permeability in fractures is similar to the rules in porous media. Diomampo et al. (2001) obtained similar experimental results through the experiments of relative permeability in fractures by nitrogen and water. So it is reasonable to use the porous media flow model to study the relative permeability in fractures (Babadagli et al., 2015).

Numerous studies have demonstrated that the flow regime will be changed by interfacial effects when fluid flows in nanotubes. Myers (2010) figured out that the interfacial effects were existed in the wall surface when the single-phase liquid flowed in nanotubes, which lead to form a thin liquid film and change flow characteristics. So there are two areas of flow pattern in nanotubes. Joseph and Aluru (2008) confirm that Myers' model is correct by molecular dynamics simulation method. Exerowa et al. (1987) and Derjaguin and Churaev (1974) studied the solid–liquid interface microscopic phenomenon further. The result shows that there are three microscopic forces between liquid and solid surfaces. Table 1 shows that they are long-range van der Waals force, double layer repulsive force and short-range structure repulsive force which are the reason of stable thin film formation on solid surface of nanotube.

For shale gas reservoirs, the main gas flow channels are natural micro-fracture spacing in 50–1500 nm normally. However these natural micro-fractures often have poor communication. After artificial hydraulic fracturing, the more penetrating fracture network is formed to benefit shale gas flow. While on the fracturing process, the formation of initial water and fracturing fluid will be in fracture network containing nanoscale pores. The fluid flow in nanoscale pores near interfaces will be affected by interfacial microstructure effects. Therefore, the interfacial effects cannot be ignored to gas-water relative permeability research in shale gas reservoirs with nanoscale pores.

In this paper we made a research in four aspects. At first, two analytical models of permeability for single phase flow considering that interfacial effect was established based on Hagen Poiseuille formula. In addition, the model of gas-water relative permeability in nanoscale pores was obtained further using capillary pressure curve. Then, we verified the tube flow model and parallel-plate flow model with classical models and experimental data, the results show that the tube flow model have good agreements with the laboratory result. Finally, the analysis of diameter, thickness of film, surface diffusion and contact angle were carried to figure out the relationship with relative permeability in nanoscale pores. The results could provide new insight and theoretical basis for shale gas reservoir production.

2. Analytical model of relative permeability

In this paper, we have used the tube flow model and the parallel-plate flow model to study the flow behavior in fracture network of shale gas reservoir with nanoscale pores. And then, the gas-water two phase permeability model was derived on the basis of the two models. Comparing with the experimental data, we could draw a conclusion about which model can describe the relative permeability more accurately in the nanoscale fracture.

2.1. Tube flow model with interfacial effects

The physical model is shown in Fig. 2. There are two flow regions in nanotube. Region 2 is the thin film with interfacial effects and region1 is bulk flow (Myers, 2010). No matter Knudsen flow or transitional flow in nanoscale pores, the interface microstructure effects are considered in Region 2 already, so fluid flow in the whole nanotube still satisfy the Hagen Poiseuille law (Prabha and Sathian, 2012).

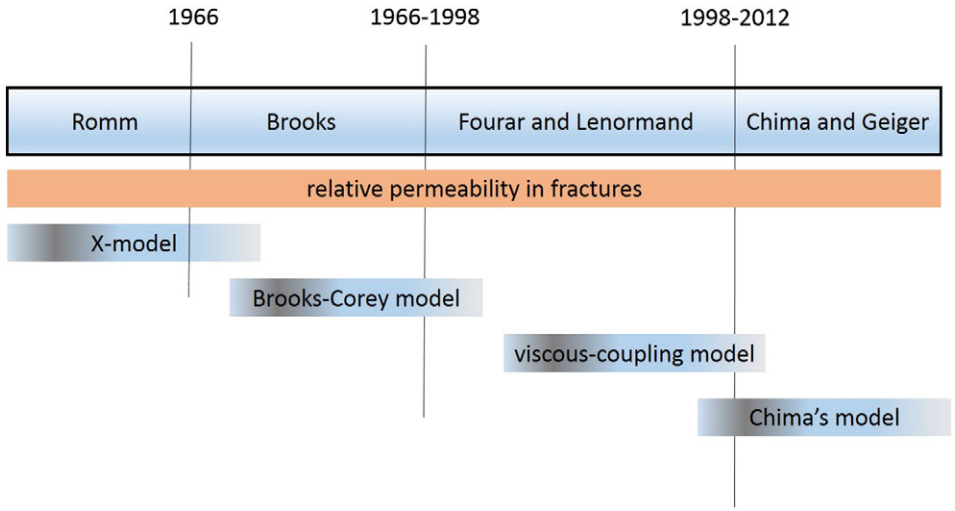

Fig. 1. Research progress of relative permeability model in fractures.

Table 1
List of the different solid-liquid molecular interactions.

Molecular interactions	Force strength	Equation of the molecular interactions
Long-range van der Waals force	Strong	$\coprod_w = -\frac{A}{6\pi h^3}$
Double layer repulsive force	Strong	$\coprod_e = -\frac{\pi\varepsilon}{8h^2}\left(\frac{kT}{eZ}\right)$
Short-range structure repulsive force	Strong	$\coprod_s = -K\ ,\exp\left(-\frac{h}{\lambda}\right)$

The velocity equations in different regions are as follows:

$$\begin{aligned} u_1(r) &= -\frac{\Delta p}{L}\frac{1}{4\mu_1}r^2 + c_1, r \in [0, R-h] \\ u_2(r) &= -\frac{\Delta p}{L}\frac{1}{4\mu_2}r^2 + c_2, r \in [R-h, R] \end{aligned} \tag{1}$$

where μ_1 and μ_2 are the viscosity of region 1 and the viscosity of region 2 in the standard state, respectively; and they satisfy the relations $\mu_2 = \alpha\mu_1$; α generally ranges from 0.6–0.8 for a hydrophobic wall, and L is the length of the nanotube.

The boundary conditions that guarantee continuity of the velocity and the shear stress and mass conservation are as follows:

$$\begin{aligned} &\frac{\partial u_1}{\partial r}(r=0) = 0 \\ &u_1(r = R-h) = u_2(r = R-h) \\ &u_1\frac{\partial u_1}{\partial r}(r = R-h) = u_2\frac{\partial u_2}{\partial r}(r = R-h) \\ &-\lambda\frac{\partial u_2}{\partial r}(r = R) = u_2(r = R) \end{aligned} \tag{2}$$

where λ is the slip length, R is the nanotube radius, and h is the thickness of region 2 that most researchers assign the value 0.7 nm (Mattia and Calabrò, 2012).

The velocity profiles derived from Eq. (1) using the boundary conditions in Eq. (2) are as follows:

$$\begin{aligned} u_1(r) &= \frac{\Delta p}{L}\frac{1}{4\mu_1}\left(R^2 - \frac{\mu_2}{\mu_1}r^2\right) + \frac{\lambda R}{2L\mu_2}\Delta p + \frac{\Delta p}{L}\frac{\mu_2-\mu_1}{4\mu_1\mu_2}(R-h)^2, r \in [0, R-h] \\ u_2(r) &= \frac{\Delta p}{L}\frac{1}{4\mu_2}\left(R^2 - r^2\right) + \frac{\lambda R}{2L\mu_2}\Delta p, r \in [R-h, R]. \end{aligned} \tag{3}$$

The velocity at the wall $u(r=R)$ can be derived as follows: $u(r = R) = \frac{\lambda R}{2\mu_2 L}\Delta p$.

Considering the influence of surface diffusion and interfacial energy, the flow velocity of the solid wall can be expressed as:

$$u(r = R) = \frac{\lambda R}{2\mu_2 L}\Delta p = \frac{U}{W_A}\Delta p \tag{4}$$

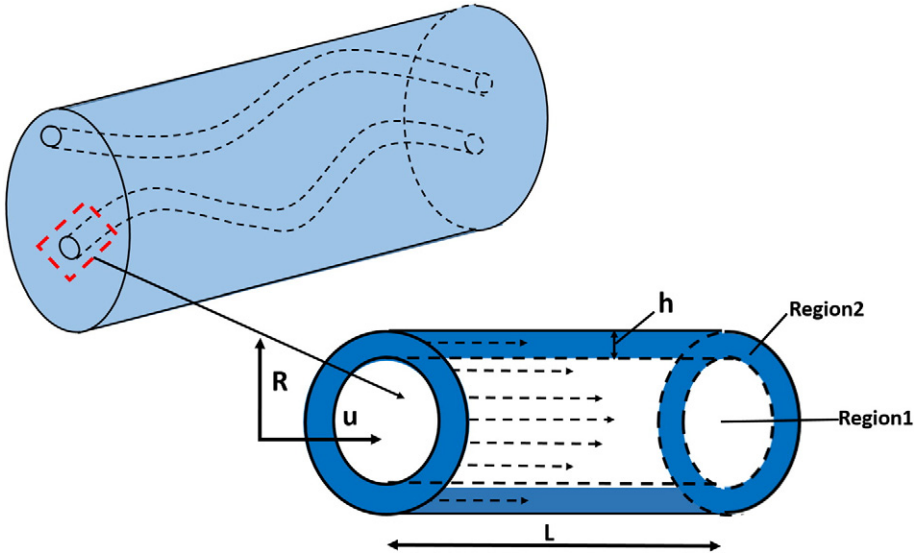

Fig. 2. Schematic of tube flow model with solid–liquid molecular interactions.

where U is surface diffusion coefficient, $U=-\frac{2\pi Rh^2}{3\mu}\frac{\partial}{\partial x}\left[\prod(h)+\gamma_{LV}\frac{\partial^2 h}{\partial x^2}\right]$, the detailed mathematical expression is given in Appendix B, and W_A is the energy per unit surface of the monolayer of the fluid molecules at the interface with the solid, which may hinder the water through the nanotubes. $W_A=\gamma_{LV}(1+\cos\theta)$,$\gamma_{LV}$ is the liquid–vapor surface tension and θ is the contact angle. Substitution of Eq. (4) into Eq. (3) yields the flow velocity expression of the two regions as

$$\begin{aligned} u_1(r)&=\frac{\Delta p}{L}\frac{1}{4\mu_1}\left(R^2-\frac{\mu_2}{\mu_1}r^2\right)+\frac{U}{W_A}\Delta p+\frac{\Delta p}{L}\frac{\mu_2-\mu_1}{4\mu_1\mu_2}(R-h)^2, r\in[0,R-h]\\ u_2(r)&=\frac{\Delta p}{L}\frac{1}{4\mu_2}\left(R^2-r^2\right)+\frac{U}{W_A}\Delta p, r\in[R-h,R]. \end{aligned} \tag{5}$$

Integrating Eq. (5), we can derive the flow equation of a nanopore as

$$Q=\int_A u dA=\int_0^{R-\delta}u_1 2\pi r dr+\int_{R-\delta}^{R}u_2 2\pi r dr \tag{6}$$

and

$$Q=\Delta p\pi\left\{\begin{array}{l}(R-h)^2\left[\frac{R^2}{4L\mu_1}+\frac{U}{W_A}-\frac{2-2\alpha+\alpha^2}{8L\alpha\mu_1}(R-h)^2\right]+\\ \left[R^2\left(\frac{R^2}{8L\alpha\mu_1}+\frac{U}{W_A}\right)-(R-h)^2\left(\frac{2R^2-(R-h)^2}{8L\alpha\mu_1}+\frac{U}{W_A}\right)\right]\end{array}\right\}$$

Define

$$\psi=(R-h)^2\left[\frac{R^2}{4L\mu_1}+\frac{U}{W_A}-\frac{2-2\alpha+\alpha^2}{8L\alpha\mu_1}(R-h)^2\right]$$

$$\zeta=R^2\left(\frac{R^2}{8L\alpha\mu_1}+\frac{U}{W_A}\right)-(R-h)^2\left(\frac{2R^2-(R-h)^2}{8L\alpha\mu_1}+\frac{U}{W_A}\right).$$

then

$$Q=\Delta p\pi(\psi+\zeta)$$

The real rock pore volume can be equivalent to the total volume of the capillaries. For the same conditions of fluid property and pressure, we assume that the nanoporous medium is constituted by nanoscale capillaries.

The porosity of the nanoporous medium ϕ is proportional to the square of the radius (Mullins and Oliver C., 2008)

$$\phi=\frac{N\pi R^2}{A} \tag{7}$$

where N is the number of capillaries, R is the nanotube radius, and A is the rock's sectional area.

According to the Dupuit–Forchheimer expression (DF expression) and Darcy's law (Tang and Cui, 2007), we obtained the seepage velocity

$$V=\frac{Q}{\phi}=\frac{K\Delta p}{\mu L}. \tag{8}$$

Considering the solid–liquid molecular interaction, the permeability can be expressed as

$$K=\frac{AL\mu(\psi+\zeta)}{NR^2} \tag{9}$$

where $\mu=\mu_1$.

However, the radius of a capillary in real rock is uneven. To simulate a practical porous medium, we assume that the pore of a low-porosity rock is constituted by different radii of nanoscale capillaries

$$Q=\sum_{i=1}^{N}\Delta p\pi N_i(\psi_i+\zeta_i) \tag{10}$$

where N_i is the number of capillaries with the radius R_i.

The porosity of the porous medium can be derived as

$$\phi=\frac{1}{A}\sum_{i=1}^{N}N_i\pi R_i^2. \tag{11}$$

According to Eqs. (9), (10) and (11), the permeability can be expressed as follows:

$$K = \mu AL \frac{\sum_{i=1}^{N} N_i(\psi_i + \zeta_i)}{\sum_{i=1}^{N} N_i R_i^2}. \tag{12}$$

From the Eq. (12), we can derive the following formula:

$$K = \mu AL \frac{\sum_{i=1}^{N} N_i \left\{ (R_i - h)^2 \frac{R_i^2}{4L\mu_1} - \frac{(1-\alpha)^2 (R_i - h)^4 - R_i^4 + 2R_i^2 (R_i - h)^2}{8L\alpha\mu_1} + R_i^2 \frac{U}{W_A} \right\}}{\sum_{i=1}^{N} N_i R_i^2}. \tag{13}$$

Define $\omega_i = \frac{R_i - h}{R_i}$.

Eq. (13) can be transformed into the following relationship

$$K = \mu AL \frac{\sum_{i=1}^{N} N_i \left\{ \frac{\omega_i^2 R_i^4}{4L\mu_1} - \frac{(1-\alpha)^2 \omega_i^4 R_i^4 - R_i^4 + 2R_i^4 \omega_i^2}{8L\alpha\mu_1} + R_i^2 \frac{U}{W_A} \right\}}{\sum_{i=1}^{N} N_i R_i^2}. \tag{14}$$

2.2. Parallel-plate flow model with interfacial effects

The physical model is shown in Fig. 3. There are two flow regions between parallel-plate. We can derive the velocity distribution equations in the parallel plate on the basis of force equilibrium. Region 4 is the thin film with interfacial effects and Region 3 is bulk flow.

The velocity equations in different regions are as follows:

$$\begin{aligned} u_3(W) &= -\frac{\Delta p}{L_1} \frac{1}{2\mu_3} W^2 + c_1, W \in \left[-\frac{1}{2} W_f + h, \frac{1}{2} W_f - h \right] \\ u_4(W) &= -\frac{\Delta p}{L_1} \frac{1}{2\mu_4} W^2 + c_2, W \in \left[-\frac{1}{2} W_f, -\frac{1}{2} W_f + h \right] \cup \left[\frac{1}{2} W_f - h_f, \frac{1}{2} W_f \right] \end{aligned} \tag{15}$$

Where u_3 and u_4 respectively are the flow velocity of region 3 and region 4; μ_3 and μ_4 are the viscosity of region 3 and the viscosity of region 4 in the standard state, respectively; and they satisfy the relations $\mu_4 = \alpha\mu_3$; αgenerally ranges from 0.6–0.8 for a hydrophobic wall; L_1 is the length of the parallel-plate; W_f is the space between the parallel-plate, and Δp is the pressure difference between the two ends of the parallel-plate.

The boundary conditions that guarantee continuity of the velocity and the shear stress and mass conservation are as follows:

$$\begin{aligned} &\frac{\partial u_3}{\partial W}(W = 0) = 0 \\ &u_3\left(W = \frac{1}{2} W_f - h\right) = u_4\left(W = \frac{1}{2} W_f - h\right) \\ &u_3 \frac{\partial u_3}{\partial W}\left(W = \frac{1}{2} W_f - h\right) = u_4 \frac{\partial u_4}{\partial r}\left(W = \frac{1}{2} W_f - h\right) \\ &-\lambda \frac{\partial u_4}{\partial W}\left(W = \frac{1}{2} W_f\right) = u_4\left(W = \frac{1}{2} W_f\right) \end{aligned} \tag{16}$$

Where λ is the slip length, and h is the thickness of region 4 that most researchers assign the value 0.7 nm.

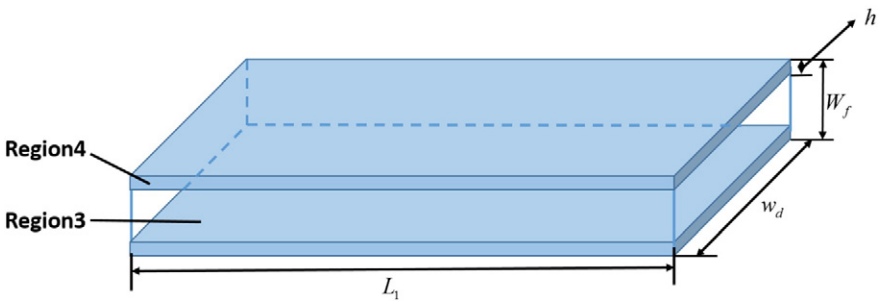

Fig. 3. Schematic of parallel-plate flow model with solid–liquid molecular interactions.

The velocity profiles derived from Eq. (15) using the boundary conditions in Eq. (16) are as follows:

$$\begin{aligned} u_3(W) &= \frac{\Delta p}{2\mu_3 L_1}\left[\left(\frac{1}{2}W_f - h\right)^2 - W^2\right] + \frac{\lambda W_f \Delta p}{2\mu_4 L_1}, W \in \left[-\frac{1}{2}W_f + h, \frac{1}{2}W_f - h\right] \\ u_4(W) &= \frac{\Delta p}{2\mu_4 L_1}\left[\left(\frac{1}{2}W_f - h\right)^2 - W^2 + \lambda W_f\right], W \in \left[-\frac{1}{2}W_f, -\frac{1}{2}W_f + h\right] \cup \left[\frac{1}{2}W_f - h_f, \frac{1}{2}W_f\right]. \end{aligned} \tag{17}$$

Considering the influence of surface diffusion and interfacial energy, the flow velocity of the parallel-plate wall can be expressed as:

$$u\left(W = \frac{1}{2}W_f\right) = \frac{\lambda W_f}{2\mu_4 L_1}\Delta p = \frac{U}{W_A}\Delta p. \tag{18}$$

Integrating Eq. (17), we can derive the flow equation as follows

$$Q_1 = \int_A u dA = \int_0^{\frac{1}{2}W_f - h} u_3 W w_d dW + \int_{\frac{1}{2}W_f - h}^{\frac{1}{2}W_f} u_4 W w_d dW \tag{19}$$

and

$$\begin{aligned} Q_1 &= \frac{(\mu_4 - \mu_3)}{8\mu_3\mu_4 L_1}\left(\frac{1}{2}W_f - h\right)^4 + \frac{\Delta p w_d W_f^2}{16\mu_4 L_1}\left[\left(\frac{1}{2}W_f - h\right)^2 - \frac{1}{8}W_f^2\right] + \frac{U}{W_A}\frac{w_d W_f^2}{8}\Delta p \\ &= \Delta p w_d\left\{\frac{(\mu_4 - \mu_3)}{8\mu_3\mu_4 L_1}\left(\frac{1}{2}W_f - h\right)^4 + \frac{W_f^2}{16\mu_4 L_1}\left[\left(\frac{1}{2}W_f - h\right)^2 - \frac{1}{8}W_f^2\right] + \frac{U}{W_A}\frac{W_f^2}{8}\right\} \end{aligned} \tag{20}$$

where w_d is the width of parallel-plate.

According to the Eqs. (7) and (8), we can derive the permeability of parallel-plate as follows:

$$\begin{aligned} K_1 &= \frac{Q_1\mu_3 L_1}{\phi_1 \Delta p} \\ K_1 &= \frac{AL\mu\left\{\frac{(\alpha-1)}{8\alpha\mu_3 L_1}\left(\frac{1}{2}W_f - h\right)^4 + \frac{W_f^2}{16\alpha\mu_3 L_1}\left[\left(\frac{1}{2}W_f - h\right)^2 - \frac{1}{8}W_f^2\right] + \frac{U}{W_A}\frac{W_f^2}{8}\right\}}{NW_f}. \end{aligned} \tag{21}$$

2.3. The models of relative permeability with interfacial effect

On the basis of Section 2.1, we could establish relative permeability model of gas-water two-phase by capillary pressure curve. And the single capillary pressure can be expressed as follows in terms of capillary pressure curve (Zhiping and Birong, 1991)

$$P_{c_i} = \frac{2\sigma\cos\theta}{R_i}. \tag{22}$$

Then

$$R_i^2 = \frac{4(\sigma\cos\theta)^2}{P_{c_i}^2}$$

And the permeability can be expressed as follows:

$$K = \mu AL\left[\frac{\sum_{i=1}^{N} N_i \frac{\omega_i{}^2(\sigma\cos\theta)^2 V_i(1-\alpha)}{P_{c_i}{}^2 L^2 \pi\mu_1} - \sum_{i=1}^{N} N_i \frac{(1-\alpha)^2\omega_i{}^4(\sigma\cos\theta)^2 V_i}{2P_{c_i}{}^2 L^2\pi\alpha\mu_1} + \sum_{i=1}^{N} N_i \frac{(\sigma\cos\theta)^2 V_i}{2P_{c_i}{}^2 L^2\pi\alpha\mu_1}}{\sum_{i=1}^{N} N_i R_i^2} + \frac{U}{W_A}\right] \tag{23}$$

$$K = \mu AL\left[\left(\frac{(1-\alpha)}{4L^2\pi\mu_1}\sum_{i=1}^{N}\omega_i{}^2 V_i\right) - \left(\frac{(1-\alpha)^2}{8L^2\pi\alpha\mu_1}\sum_{i=1}^{N}\omega_i{}^4 V_i\right) + \left(\frac{1}{8L^2\pi\alpha\mu_1}\sum_{i=1}^{N} V_i\right) + \frac{U}{W_A}\right]. \tag{24}$$

When the number i root canal is filled with liquid, the saturation satisfy $S_i = \frac{V_i}{V_p}$, then $V_p = \frac{V_i}{S_i}$. Because of the volume of the sample meet the formula $V = AL$, so the rock porosity is expressed as below:

$$\phi = \frac{V_p}{AL} = \frac{V_i/S_i}{AL}.$$

Then: $V_i = \phi AL S_i$.

The Eq. (24) is transformed into an integral form:

$$K=\frac{(1-\alpha)}{4\pi}\phi A^2\sum_{i=1}^{N}\omega_i{}^2S_i-\frac{(1-\alpha)^2}{8\pi\alpha}\phi A^2\sum_{i=1}^{N}\omega_i{}^4S_i+\frac{\phi A^2}{8\pi\alpha}\sum_{i=1}^{N}S_i+\mu AL\frac{U}{W_A} \tag{25}$$

$$K=\frac{(1-\alpha)}{4\pi}\phi A^2\int_0^1\omega_i{}^2dS_i-\frac{(1-\alpha)^2}{8\pi\alpha}\phi A^2\int_0^1\omega_i{}^4dS_i+\frac{\phi A^2}{8\pi\alpha}\int_0^1dS_i+\mu AL\frac{U}{W_A}. \tag{26}$$

The effective permeabilities of gas-water two-phase were respectively indicated as:

$$K_{rwt}=\frac{(1-\alpha)}{4\pi}\phi A^2\int_0^{s_i}\omega_i{}^2dS_i-\frac{(1-\alpha)^2}{8\pi\alpha}\phi A^2\int_0^{s_i}\omega_i{}^4dS_i+\frac{\phi A^2}{8\pi\alpha}\int_0^{s_i}dS_i+\mu AL\frac{U}{W_A} \tag{27}$$

$$K_{rgt}=\frac{(1-\alpha)}{4\pi}\phi A^2\int_{s_i}^1\omega_i{}^2dS_i-\frac{(1-\alpha)^2}{8\pi\alpha}\phi A^2\int_{s_i}^1\omega_i{}^4dS_i+\frac{\phi A^2}{8\pi\alpha}\int_{s_i}^1dS_i+\mu AL\frac{U}{W_A}. \tag{28}$$

And the relative permeability can be respectively expressed as:

$$K_{rw}=\frac{\frac{(1-\alpha)}{4\pi}\phi A^2\int_0^{s_i}\omega_i{}^2dS_i-\frac{(1-\alpha)^2}{8\pi\alpha}\phi A^2\int_0^{s_i}\omega_i{}^4dS_i+\frac{\phi A^2}{8\pi\alpha}\int_0^{s_i}dS_i+\mu AL\frac{U}{W_A}}{\frac{(1-\alpha)}{4\pi}\phi A^2\int_0^1\omega_i{}^2dS_i-\frac{(1-\alpha)^2}{8\pi\alpha}\phi A^2\int_0^1\omega_i{}^4dS_i+\frac{\phi A^2}{8\pi\alpha}\int_0^1dS_i+\mu AL\frac{U}{W_A}} \tag{29}$$

$$K_{rg}=\frac{\frac{(1-\alpha)}{4\pi}\phi A^2\int_{s_i}^1\omega_i{}^2dS_i-\frac{(1-\alpha)^2}{8\pi\alpha}\phi A^2\int_{s_i}^1\omega_i{}^4dS_i+\frac{\phi A^2}{8\pi\alpha}\int_{s_i}^1dS_i+\mu AL\frac{U}{W_A}}{\frac{(1-\alpha)}{4\pi}\phi A^2\int_0^1\omega_i{}^2dS_i-\frac{(1-\alpha)^2}{8\pi\alpha}\phi A^2\int_0^1\omega_i{}^4dS_i+\frac{\phi A^2}{8\pi\alpha}\int_0^1dS_i+\mu AL\frac{U}{W_A}}. \tag{30}$$

Considering the tortuosity of the actual rock hole, the gas-water relative permeability can be expressed as:

$$K_{rw}=(t_{rw})^2\frac{\frac{(1-\alpha)}{4\pi}\phi A^2\int_0^{s_i}\omega_i{}^2dS_i-\frac{(1-\alpha)^2}{8\pi\alpha}\phi A^2\int_0^{s_i}\omega_i{}^4dS_i+\frac{\phi A^2}{8\pi\alpha}\int_0^{s_i}dS_i+\mu AL\frac{U}{W_A}}{\frac{(1-\alpha)}{4\pi}\phi A^2\int_0^1\omega_i{}^2dS_i-\frac{(1-\alpha)^2}{8\pi\alpha}\phi A^2\int_0^1\omega_i{}^4dS_i+\frac{\phi A^2}{8\pi\alpha}\int_0^1dS_i+\mu AL\frac{U}{W_A}} \tag{31}$$

$$K_{rg}=(t_{rg})^2\frac{\frac{(1-\alpha)}{4\pi}\phi A^2\int_{s_i}^1\omega_i{}^2dS_i-\frac{(1-\alpha)^2}{8\pi\alpha}\phi A^2\int_{s_i}^1\omega_i{}^4dS_i+\frac{\phi A^2}{8\pi\alpha}\int_{s_i}^1dS_i+\mu AL\frac{U}{W_A}}{\frac{(1-\alpha)}{4\pi}\phi A^2\int_0^1\omega_i{}^2dS_i-\frac{(1-\alpha)^2}{8\pi\alpha}\phi A^2\int_0^1\omega_i{}^4dS_i+\frac{\phi A^2}{8\pi\alpha}\int_0^1dS_i+\mu AL\frac{U}{W_A}} \tag{32}$$

where: $t_{rw}=\frac{S_i-S_{\min}}{1-S_{\min}}$

$$t_{rg}=\frac{1-S_{i-}S_{\mathrm{og}}}{1-S_{\min}-S_{\mathrm{og}}}.$$

Also, we can derive the gas-water two phase relative permeability of parallel-plate flow model with the same method. Firstly, the permeability of parallel-plate can be derived from Eq. (21) as follows.

$$K_1=\frac{AL_1\left\{\frac{\omega_1^4(\alpha-1)}{128\alpha L_1w_d^3}\left(\pi R_d^2\right)^3+\frac{\left(\pi R_d^2\right)^3}{64\alpha L_1w_d^3}\left[\omega_1^2-\frac{1}{2}\right]+\frac{U}{W_A}\frac{\mu_3\pi R_d^2}{8w_d}\right\}}{N} \tag{33}$$

where: $\omega_1=\frac{\frac{1}{2}W_f-h}{\frac{1}{2}W_f}=\frac{W_f-2h}{W_f}$.

Then, we can obtain the gas-water two phase relative permeability of parallel-plate flow model.

$$K_{1rw}=(t_{1rw})^2\frac{\frac{\phi A^2}{128\alpha L_1^2w_d^3}\int_0^{s_i}\left\{\omega_{1i}^4(\alpha-1)+2\left(\pi R_d^2\right)^3\left[\omega_{1i}^2-\frac{1}{2}\right]\right\}dS_{1i}+\int_0^{s_i}\frac{U\phi A^2L_1}{8W_Aw_d}dS_{1i}}{\frac{\phi A^2}{128\alpha L_1^2w_d^3}\int_0^1\left\{\omega_{1i}^4(\alpha-1)+2\left(\pi R_d^2\right)^3\left[\omega_{1i}^2-\frac{1}{2}\right]\right\}dS_{1i}+\int_0^1\frac{U\phi A^2L_1}{8W_Aw_d}dS_{1i}} \tag{34}$$

$$K_{1rg} = (t_{1rg})^2 \frac{\frac{\phi A^2}{128\alpha L_1^2 w_d^3}\int_{s_i}^{1}\left\{\omega_{1i}^4(\alpha-1)+2\left(\pi R_d^2\right)^3\left[\omega_{1i}^2-\frac{1}{2}\right]\right\}dS_{1i}+\int_{s_i}^{1}\frac{U\phi A^2 L_1}{8W_A w_d}dS_{1i}}{\frac{\phi A^2}{128\alpha L_1^2 w_d^3}\int_{0}^{1}\left\{\omega_{1i}^4(\alpha-1)+2\left(\pi R_d^2\right)^3\left[\omega_{1i}^2-\frac{1}{2}\right]\right\}dS_{1i}+\int_{0}^{1}\frac{U\phi A^2 L_1}{8W_A w_d}dS_{1i}} \tag{35}$$

where: $t_{1rw}=\frac{S_i-S_{\min}}{1-S_{\min}}$, $t_{1rg}=\frac{1-S_i-S_{og}}{1-S_{\min}-S_{og}}$.

3. Results and discussion

Researchers have studied the flow characteristics of water through the nanotubes by means of molecular dynamics simulation. (Thomas and McGaughey, 2009) And there is little research on the two phase flow in the nanotubes. In the actual shale reservoir, after fracturing, the shale fracture network scale is from 50 nm to 50 μm. Because of the limitation of the experimental conditions, the relative permeability in the nanoporous was not determined experimentally. Current experimental conditions can only satisfy the micro-scale experiment of relative permeability. In this paper, we compare the relative permeability experimental result in Table 2 (Chen, Chih Ying et al., 2004) with the classical model and the present model under the same condition (R = 0.1 μm, S_{wc} = 0.2, ΔP = 7.5 Mpa).

3.1. Model validation

Fig. 4 compares the experimentally measured relative permeability ratio curves for gas and water (blue points) with the relative permeability ratio curves estimated from Brooks–Corey model (λ = infinite, S_{wc} = 0.2), Chima's model, Kozeny–Carman equation and present models (S_{wc} = 0.2). It is apparent that the flow models with interfacial effects match the experimental data better than without interfacial effects.

The result shows that the present model can reflect the effect of the interfacial effects on the relative permeability more accurately. When water saturation is less than isotonic point S_w = 0.4 from Fig. 4, the relative permeability ratio with interfacial effects is lower than not with interfacial effects which are positive for gas flow. On the contrary, when water saturation is higher than isotonic point, the relative permeability ratio with interfacial effects is higher than not with interfacial effects which are positive for gas flow because of existence of surface diffusion.

Table 2
The experimental data of relative permeability.

S_w (dimensionless)	krg (dimensionless)	krw (dimensionless)	Krg/krw (dimensionless)
0.2013	0.86	0.0054	358.33
0.2148	0.82	0.014	58.57
0.2216	0.69	0.053	13.019
0.2762	0.56	0.096	5.833
0.3445	0.42	0.135	3.11
0.4067	0.34	0.162	2.099
0.5024	0.186	0.185	1.005
0.5793	0.165	0.26	0.635
0.6321	0.121	0.34	0.356
0.6538	0.053	0.41	0.129
0.6915	0.0092	0.52	0.0177

3.2. Effect of nanotube radius

Fig. 5 is relative permeability curves with different nanotube radius. It shows that the larger the nanotube radius, the greater the relative permeability values under the same water saturation. Because with increasing nanoscale diameters, the interfacial microstructure effect and the resistance of fluid flow are both decreasing. Fluid flow more smoothly, thereby the gas-water two-phase relative permeability increases.

3.3. Effect of thicknesses of films

Fig. 6 is relative permeability curves with different thicknesses of films. With increasing film thickness, the fluid velocity decreases in spreading solid surface so that surface diffusion coefficient decreases and flow resistance increases in nanoscale pores. It is apparent that relative permeability curves move down and the gas-water two-phase relative permeability decreases.

3.4. Effect of surface diffusion

Fig. 7 is relative permeability curves with different surface diffusions. With increasing surface diffusion, the fluid velocity increases in spreading solid surface so that flow resistance decreases in nanoscale pores. It is apparent that relative permeability curves move up with increasing surface diffusion and the gas-water two-phase relative permeability increases too.

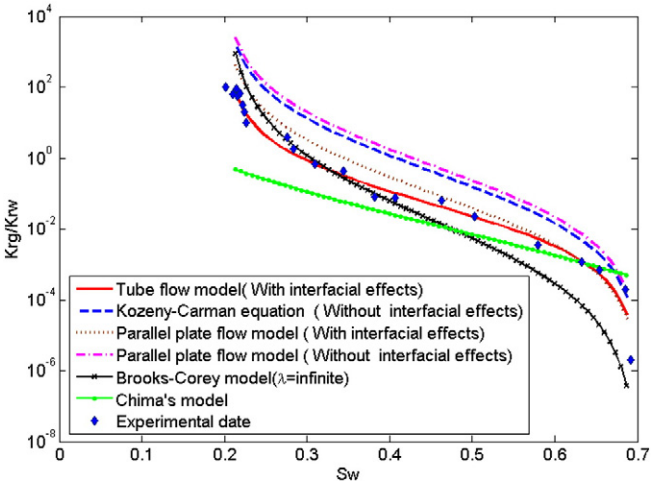

Fig. 4. Comparison of laboratory measurement data (green points) with Brooks–Corey model, Chima's model, Kozeny–Carman equation and present models.

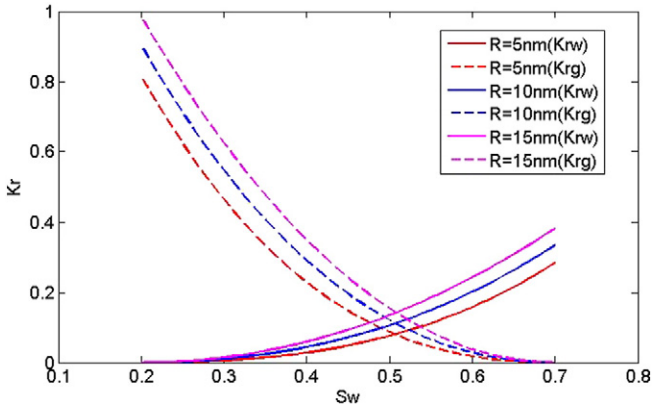

Fig. 5. Relative permeability curves with different nanotube radius.

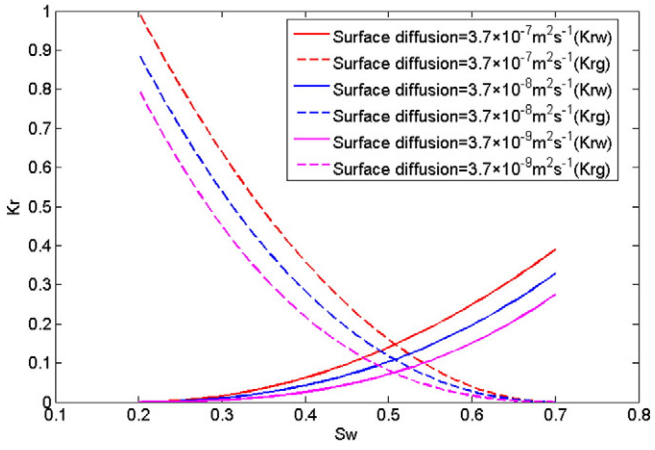

Fig. 7. Relative permeability curves with different surface diffusions.

3.5. Effect of contact angle

Fig. 8 is relative permeability curves with different contact angles. With increasing contact angle, the solid–liquid interface energy decreases and the hydrophobic properties of surfaces increase which leads to flow resistance decreases in nanoscale pores. The microscopic force is gradually reduced and interfacial effects are changed from negative to positive. The gas-water two-phase relative permeability increases with increasing contact angle too.

From Fig. 9 we can find that interfacial effects include two effects. One is surface diffusion the other is wettability. As we all know surface diffusion plays a positive role to promote fluid flow. At the same time, when the contact angle >90° solid interface repel water and the hydrophobic of surfaces reduce the resistance to fluid flow. On the contrary when contact angle <90°, the solid interface shows hydrophilic properties which play a negative effect to the fluid flow. The interfacial effects cannot be ignored for relative permeability and production evaluation in shale gas reservoirs containing nanoscale pores.

4. Conclusion

The interfacial effects include two effects. One is surface diffusion, the other is wettability. A new gas-water relative permeability model with interfacial effects was established in terms of Hagen Poiseuille formula and capillary pressure curve. Then, we verified the tube flow model and parallel-plate flow model with classical models and experimental data, the results show that the tube flow model has good agreements with the laboratory result. Based on the tube flow model, the changing characteristics of gas-water relative permeability under different conditions were analyzed after calculations.

The results show that the larger the nanotube radius, the greater relative permeability values under the same water saturation because of decreasing both interfacial microstructure effect and the resistance of fluid flow. With the increasing of film thickness, the fluid velocity decreases in spreading solid surface and surface diffusion coefficient decreases in nanoscale pores. When the contact angle >90° solid interface repel water and the hydrophobic of surfaces reduce the resistance to fluid flow, and the gas-water relative permeability increases with increasing contact angle. On the contrary when contact angle <90°, the solid interface shows hydrophilic properties which play a negative effect to the fluid flow.

This study has provided a new insight and theoretical basis for development of shale gas reservoirs with nanoscale pores.

Acknowledgements

We gratefully acknowledge the Major State Basic Research Development Program of China under Grant No. 2013CB228002, the National Nature Science Foundation of China under Grant 41303059 and 51404024, and the Beijing Higher Education Young Elite Teacher Project under Grant No. 2013012601601 for financial support.

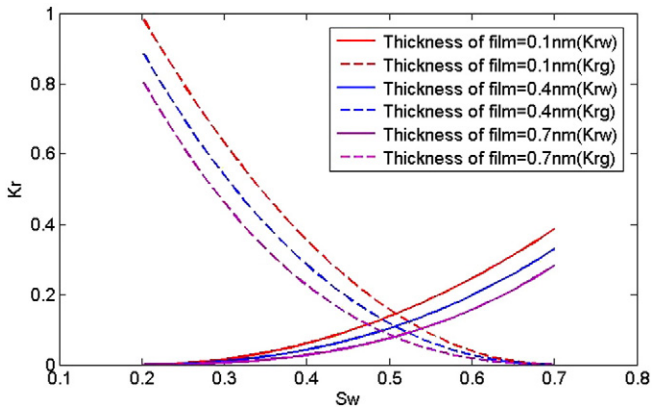

Fig. 6. Relative permeability curves with different thicknesses of films.

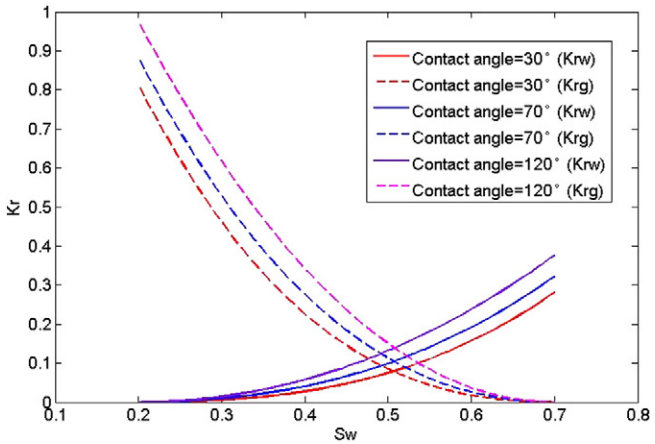

Fig. 8. Relative permeability curves with different contact angles.

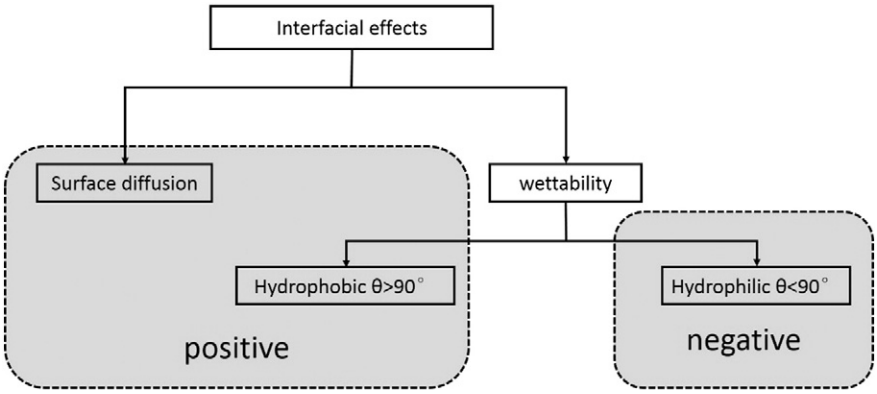

Fig. 9. Schematic diagram of interfacial effects.

Appendix A. The classical relative permeability models of fractures

The relative permeability functions are the most common and useful methods for understanding flow mechanisms and predicting petroleum recovery in fractures and porous media. Since 1950s, many scholars have done a lot of research on the relative permeability in fractures based on the practical production and the classical theory. And a series of theoretical and semi-empirical models for calculating relative permeability have been derived. The classical relative permeability models are as follows:

A.1. Romm's model

$$K_{rw} = S_w, K_{rg} = S_g \quad \text{and} \quad K_{rw} + K_{rg} = 1.$$

A.2. Brooks' model

$$K_{rw} = \left(S_w^*\right)^{(2+3\lambda)/\lambda}$$

$$K_{rg} = \left(1-S_w^*\right)^2\left[1-\left(S_w^*\right)^{(2+\lambda)/\lambda}\right]$$

where: $S_w^* = \frac{S_w - S_{wc}}{1-S_{wc}-S_{gc}}$.

A.3. Viscous-coupling model

$$K_{rw} = \frac{S_w^2}{2}(3-S_w)$$

$$K_{rg} = (1-S_w) + \frac{3}{2}\mu_r S_w(1-S_w)(2-S_w)$$

where: $\mu_r = \mu_g/\mu_w$.

A.4. Chima's model

$$K_{rw} = S_w^2\frac{\left(2S_w^2 + 3S_gS_w\right)}{2}$$

$$K_{rg} = S_g^2\left(\frac{2S_g^2 + 3\mu_r S_w^2 + 6\mu_r S_g S_w}{2}\right)$$

where: $\mu_r = \mu_g/\mu_w$.

Appendix B. The solid–liquid molecular interactions

The spreading of an aqueous film on a solid surface is very important in many industrial applications such as surface modification, heat transfer and enhanced oil recovery. In nanotubes, considering the intermolecular interaction, the spreading is a leading effect to promote fluid flow. And when the liquid is non-volatile, the principle of spreading effect is surface diffusion. The dynamic equation is as follows:

$$U = -\frac{2\pi R h^2}{3\mu}\frac{\partial}{\partial x}\left[\prod(h) + \gamma_{LV}\frac{\partial^2 h}{\partial x^2}\right]$$

Where $\prod(h)$ is the surface tension gradient of the film, and the numerical value satisfies the following relational expression: $\prod(h) = \prod_w + \prod_e + \prod_s$, $\prod_w$ is the long-range van der Waals forces between the solid–liquid molecular interactions (Derjaguin and Landau, 1993), $\prod_e$ is the double-layer repulsive force (Derjaguin and Churaev, 1974) and $\prod_s$ is the short-range structure repulsive force (Exerowa et al., 1987). Their expressions are expressed as

$$\prod_w = -\frac{A}{6\pi h^3}, \prod_e = -\frac{\pi\varepsilon}{8h^2}\left(\frac{kT}{eZ}\right), \prod_s = -K_d\exp\left(-\frac{h}{\delta}\right)$$

where A is the Hamaker constant, which characterize the size of the van Edward attraction between different materials, ε is the water dielectric constant, k is the Boltzmann constant; e is the electric quantity of elementary charge, T is the thermodynamic temperature of 20 °C, Z is the ion valence, K_d is the constant of structural force for water, and δ is the attenuation length. The parameter values are shown in Table 3.

Table 3
Parameter list for the spreading effect.

Parameter	Value	Parameter	Value
ε (F/m)	80.18	Z	2
k (J/K)	1.38×10^{-23}	K_d (N/m^2)	1.64×10^{10}
e(C)	1.6×10^{-19}	δ (nm)	1.2
T(K)	293.16	γ_{LV} (mN/m)	59.763
A(J)	4×10^{-20}		

References

Babadagli, T., Raza, S., Ren, X., Develi, K., 2015. Effect of surface roughness and lithology on the water-gas and water-oil relative permeability ratios of oil-wet single fractures. Int. J. Multiphase Flow.

Beskok, A., Karniadakis, G.E., Trimmer, W., 1996. Rarefaction and compressibility effects in gas microflows. J. Fluids Eng. 118 (3), 448–456.

Brooks, R.H., 1966. Properties of porous media affecting fluid flow. J. Irrig. Drain. Div.Proc. Am. Soc. Civ. Eng. 92, 61–88.

Chen, Chih Ying, Horne, R.N., Fourar, M., 2004. Experimental study of liquid-gas flow structure effects on relative permeabilities in a fracture. Water Resour. Res. 40, 474–480.
Chima, A., Geiger, S., 2012. An analytical equation to predict gas/water relative permeability curves in fractures. SPE Latin America and Caribbean Petroleum Engineering Conference. Society of Petroleum Engineers (January).
Corey, A.T., 1954. The interrelation between gas and oil relative permeabilities. Prod.Mon. 19 (1), 38–41.
Derjaguin, B.V., Churaev, N.V., 1974. Structural component of disjoining pressure. J. Colloid Interface Sci. 49 (2), 249.
Derjaguin, B., Landau, L., 1993. Theory of the stability of strongly charged lyophobic sols and of the adhesion of strongly charged particles in solutions of electrolytes. Prog. Surf. Sci. 43 (1), 30–59.
Diomampo, G., Chen, C.Y., Li, K., Horne, R.N., 2001. Relative permeability through fractures. Proceedings of the 27th Workshop on Geothermal Reservoir Engineering, pp. 28–30 (August).
Exerowa, D., Kolarov, T., Khristov, Khr, 1987. Direct measurement of disjoining pressure in black foam films. I. Films from an ionic surfactant. Colloids Surf. 22 (2), 161–169.
Fourar, M., Lenormand, R., 1998. A viscous coupling model for relative permeabilities in fractures. SPE 49006, 27–30.
Haifeng, Z., Mian, C., Yan, J., Yunhong, D., Yonghui, W., 2012. Rock fracture kinetics of the fracture mesh system in shale gas reservoirs. Pet. Explor. Dev. 39 (4), 465–470.
Joseph, S., Aluru, N.R., 2008. Why are carbon nanotubes fast transporters of water? Nano Lett. 8 (2), 452–458.
Mattia, D., Calabrò, F., 2012. Explaining high flow rate of water in carbon nanotubes via solid–liquid molecular interactions. Microfluid. Nanofluid. 13 (1), 125–130.
Mullins, Oliver, C., 2008. The Physics of Reservoir Fluids: Discovery Through Downhole Fluid Analysis. Schlumberger.
Myers, T., 2010. Why are slip lengths so large in carbon nanotubes? Microfluid. Nanofluid. 10 (5), 1141–1145.
Ozkan, E., Raghavan, R.S., Apaydin, O.G., 2010. Modeling of fluid transfer from shale matrix to fracture network. In SPE Annual Technical Conference and Exhibition. Society of Petroleum Engineers (January).
Persoff, P., Pruess, K., 1995. Two-phase flow visualization and relative permeability measurements in natural rough-walled rock fractures. Water Resour. Res. 3 (5), 1175–1186.
Prabha, S.K., Sathian, S.P., 2012. Molecular-dynamics study of Poiseuille flow in a nanochannel and calculation of energy and momentum accommodation coefficients. Phys. Rev. E 85 (4), 041201.
Romm, E.S., 1966. Fluid Flow in Fractured Rocks. Nedra Publishing House, Moscow (English translation, W.R. Balke, Bartlesville, OK, 1972).
Tang, H.J., Cui, K.H., 2007. Reservoir Physics. Petroleum industry, Beijing.
Thomas, J.A., McGaughey, A.J., 2009. Water flow in carbon nanotubes: transition to subcontinuum transport. Phys. Rev. Lett. 102 (18), 184502.
Yang, F., Ning, Z.F., Hu, C.P., Wang, B., Peng, K., Liu, H.Q., 2013. Characterization of microscopic pore structures in shale reservoirs. Acta Pet. Sin. 34 (2), 301–311.
Zhiping, Li, Birong, Zhao, 1991. The capillary pressure curve calculation method of gas water two phase relative permeability curve and calculating program. Drill. Prod. Technol. 01, 46–51.